An Indirect Method and Equipment for Temperature Monitoring and Control

Radu ETZ[1], Dorin PETREUS[1], Tiberiu FRENTIU[2], Toma PATARAU[1], Cristian ORIAN[1]
[1]*Technical University of Cluj-Napoca, 400114, Romania*
[2]*Babes-Bolyai University, Cluj-Napoca, 400028,Romania*
radu.etz@ael.utcluj.ro

***Abstract*—A new temperature control method for a metallic filament used at high temperature values is proposed by the authors in this paper. The filament used is heated by a switch mode power supply built around a step-down converter. The method uses a microcontroller that implements the temperature control algorithm and also the power supply control loops. The temperature is controlled using a proposed new algorithm based on the output current and output voltage measurements of the power supply already available for implementing the average current mode control. In this way the resistance of the filament can be determined and controlled in a resistance feedback loop. The proposed algorithm will control the resistor value corresponding to the required temperature. The reference resistance value is computed based on the temperature-resistance characteristic of the filament each time a new temperature is introduced in dedicated computer software on a PC. The value is transmitted to the microcontroller via USB interface. The temperature control algorithm and experimentally results are presented in detail in the paper.**

***Index Terms*—DC-DC power converters, digital control, microcontrollers, negative feedback, temperature control.**

I. INTRODUCTION

Soil, food and other type of samples need to be vaporized for optical spectrometry analysis. Vaporization is one of the applications where the presented control algorithm can be used. The metal atomizers [1] and graphite furnaces [2] have been widely studied as means of sample introduction in plasma optical spectrometry equipment [3-5]. The graphite furnaces can be very expensive because a high purity carbon material is required and mass production cannot be applied. Carbon depositing on the torch and the bulky elaborated power supplies [6] can also be mentioned as disadvantages of using graphite furnaces. The metal atomizers based on tungsten [7, 8] and other metallic materials proved more adequate for electro thermal vaporization (ETV) in mobile equipment [9, 10]. The small size of such devices allows sample volumes of microliters and higher heating rates can be employed using lower power supply compared to graphite furnaces [11]. For example the ETV device and the other equipment can be supplied from a car battery [12].

For temperature control two distinct devices can be used, one for sensing and the other for heating purposes or as demonstrated in [13] only a single resistor can be used for both purposes. A problem can be identified when using metallic coils because the temperature sensors required are generally bulky and expensive and even if the dimension is not an issue, they can act as heatsinks for the thin metallic wire. Methods for controlling the metallic coil temperature can be found in literature based on the voltamperometric method [14]. Based on this method an electro thermal vaporizer using a constant current source is presented in [15] and in [16] a computer program used to control the current range of the supply is introduced. Using the same principle a method that measures the voltage drop on the metallic coil with a sampling period and computes its slope in order to determine when the filament is dry is presented in [17]. In order to implement these types of temperature control many researchers make use of commercial DC power supplies [18] that are redesigned for intelligent control. When using the voltamperometric method without a feedback loop, the current supplied from the power supply does not change if the operating parameters such as the gas flow in the equipment change in time. This disadvantage is eliminated when using the new method proposed by the authors in this paper. The proposed method does not need a dedicated temperature sensor because it computes the temperature indirectly using the filament resistance determined based on the measured current and voltage.

The new method proposed by the authors in this paper is an indirect one based on the experimental results used to compute the resistance, voltage or current characteristics versus temperature of a metallic filament. One method of implementation is using look up tables [19]. This method is good for applications where the operating parameters are not changing. In the mobile spectrometry equipment the ETV takes place in argon. The gas flow speed can change, affecting the temperature of the filament. In this case the method based on look up tables is not adequate and an active control algorithm must be used.

II. THE PROPOSED TEMPERATURE CONTROL ALGORITHM

In order to present the operating principle a block schematic, Fig. 1, of the indirect temperature control system has been constructed. The microcontroller is used to implement the temperature control algorithm and the average current mode control (ACMC) used to control the power delivered by the power supply. ACMC has two control loops, the voltage and current loop, and their corresponding data must be computed under 10 μs for a 100kHz switching frequency. This is why the resistance reference is computed on a PC in order to minimize the unnecessary processing load.

This work was supported by a grant of the Romanian National Authority for Scientific Research, CNDI–UEFISCDI, project number PN-II-PT-PCCA-2011-3.2-0219 (Contract no. 176/2012).

Digital Object Identifier 10.4316/AECE.2015.04012

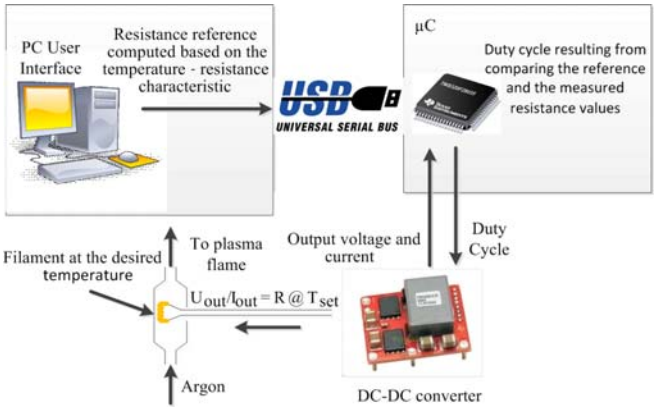

Figure 1. The block schematic

In order to implement the indirect temperature control algorithm the following methodology is proposed: 1) The voltage on the filament and current through it are measured. 2) Based on these two measurements the filament resistance at the corresponding sampling period is computed. 3) Taking into account that the filament resistance depends on temperature, by imposing the power delivered from the power supply, the temperature can be controlled. Using this methodology, the temperature is controlled indirectly maintaining the filament resistance at the value corresponding to the prescribed filament temperature Fig. 2. The prescribed filament resistance, R_{ref}, is computed using the filament resistance-temperature equation. The significance of R_{init} is the resistance of the filament during the initial steady state before the reference is changed to a new value, that corresponds to the required temperature.

R_{ref} is computed using a PC where the dedicated control user interface is installed and then it is transmitted to the microcontroller where the control algorithm is implemented.

The process variable in this case is the filament resistance, but the value that is changed at each algorithm step in case the steady state has not been reached is the voltage on the filament.

The operating principle of the algorithm is presented for the two possible cases: $R_{ref}>R_{filament}$ and $R_{ref}<R_{filament}$, where R_{ref} is the filament resistance reference value determined for a required temperature based on the temperature resistance equation and $R_{filament}$ is the resistance of the filament computed each algorithm step based on the sampled current and voltage values. For the first case after computing the $R_{filament}=U/I$ value and comparing it to R_{ref} the voltage reference will be incremented with a step. In the second case when $R_{ref}<R_{filament}$, the reference voltage will be decremented. The comparison continues and the incrementing/decrementing process is executed with the tracking algorithm period until the equality relation between R_{ref} and $R_{filament}$ is achieved.

The step value is chosen in correlation with the imposed dynamic performances and the thermal inertia of the filament. This value is in close connection with the algorithm step period. If the period has a small value and the algorithm step is large the loop will be fast but oscillations can appear and can lead to instability.

III. Power Stage Implementation

As presented in Fig. 1, power is supplied to the filament from a DC-DC converter. The power supply needs to have high efficiency, small size and communication capabilities [20]. Because of these limitations the power stage is implemented using digital control [21, 22].

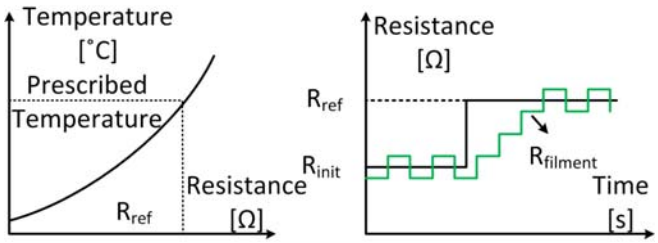

Figure 2. a) The temperature resistance dependency graphically represented. b) The filament resistance $R_{filament}$ waveform when a reference step resistance is applied.

The conventional method for designing a negative feedback control loop is usually applied to linear time invariant systems (LTI). Switch mode power supplies (SMPS) are not LTI systems but they can be modeled as linear and invariant systems using approximations. Because of the approximations the system dynamics will be affected but being aware of this disadvantage the designer can take them into account during the development stage and take some measures [23].

Nonlinearities in a step down converter can be mentioned as the effect of the switch-mode functionality, the voltage and current ripple and the passive components temperature drift. Small signal models [24] can be created for different control methods in order to linearize the system. The control method used for the vaporizer power supply is the average current mode control. The small signal model for this control method is presented in Fig. 3. This control method implies two control loops: a fast inner current loop and a slow voltage loop that gives the reference for the first loop.

The symbol ˆ in Fig. 3 refers to a small variation in the signal and d- the duty cycle, V_g- the converter supply voltage, V_o- the output voltage, I_c- the current reference, ε_i- the current loop error signal, u_i- the command signal, I_L- the average inductor current.

The resulting transfer function for the model in Fig. 3 is presented in (1).

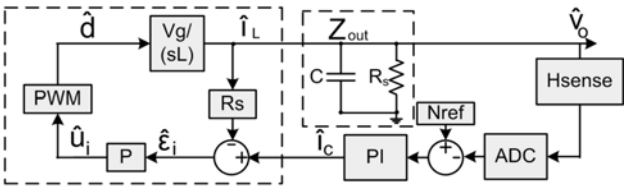

Figure 3. Small signal model for the average current mode control step down converter.

$$G_{vc}(s)=\left.\frac{\hat{v}_o(s)}{\hat{i}_c(s)}\right|_{\hat{v}_g=0}=\frac{R\cdot(1+s\cdot ESR\cdot C)}{1+s\cdot(R+ESR)\cdot C} \quad (1)$$

Where ESR is the parasitic series resistance of the output capacitor. Analyzing (1) one can see that the transfer function is of first order one compared to voltage mode control where the transfer function is of second order. This is possible because when using the average current mode control the information about the inductor current is used in the inner current loop.

The DC-DC converter used is a synchronous step down converter. The synchronous topology [25] has a higher efficiency than the standard topology and can also sink current (the discontinuous conduction mode is eliminated). The two control loops, Fig. 9, needed by the average current mode control method are first designed in the analog domain and then transposed in discrete domain using the Z transform.

The transformation process from Laplace domain to Z domain introduces supplementary delays affecting the phase margin. These delays were taken into account during the design of the digital control loops. Other delays that affect the digital implementation can be identified as the delays introduced by the converters and the processor computational limitations. The analog to digital converter (ADC) introduces a delay caused by the sampling and conversion process and the time needed by the processor to compute the new duty cycle value is also of great importance even if the coefficients are in fix point representation and the assembly language is used to implement the control algorithm. These delays are mainly determined by the operating frequency and the architecture of the controller used. The summation of all the delays introduced by the discrete implementation of the control algorithm limits the switching frequency maximum value. The delays summation must be lower than a switching period for a controller that updates its output each switching period. For a clock frequency of 60MHz on the 320F28027 microcontroller from Texas Instruments (TI), 725ns were obtained for the time needed to implement a proportional-integral (PI) controller and 1 us for the conversion time of two analog channels resulting a total time of 2.45us. This limits the switching frequency to 400KHz. For the vaporizer implementation a 100KHz switching frequency was chosen. From Fig. 4 one can observe that even if the samples are taken at half the switching period, there still is enough time to compute the new duty cycle value. BG refers to the background loop needed to perform the incremental temperature algorithm and the communication protocol with the decision processes associated and ISR refers to the ADC interrupt service routine.

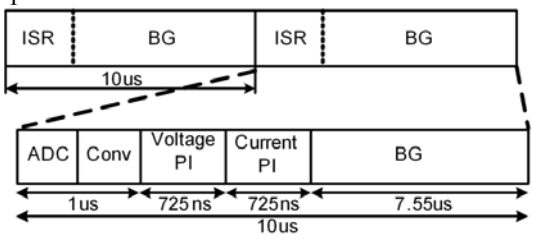

Figure 4. The time needed by sampling, conversion and two PI controllers relative to one switching period for the vaporizer device.

The first step in order to implement the incremental temperature algorithm when referring to the power stage is to design the two PI control loops used in the average current mode control method for the step down converter. The average current mode control method acts in order for the converter to deliver the power needed by the filament to reach the desired prescribed temperature value. To implement the control algorithm both the current and voltage loops are active. The samples for the inductor current and output voltage are taken at half of the duty cycle in order to measure the average value.

For the simulation results the two digital control loops were implemented in a generic microcontroller along with the ADC. In Fig. 5 the simulation results are presented and in Fig. 6 the experimental results.

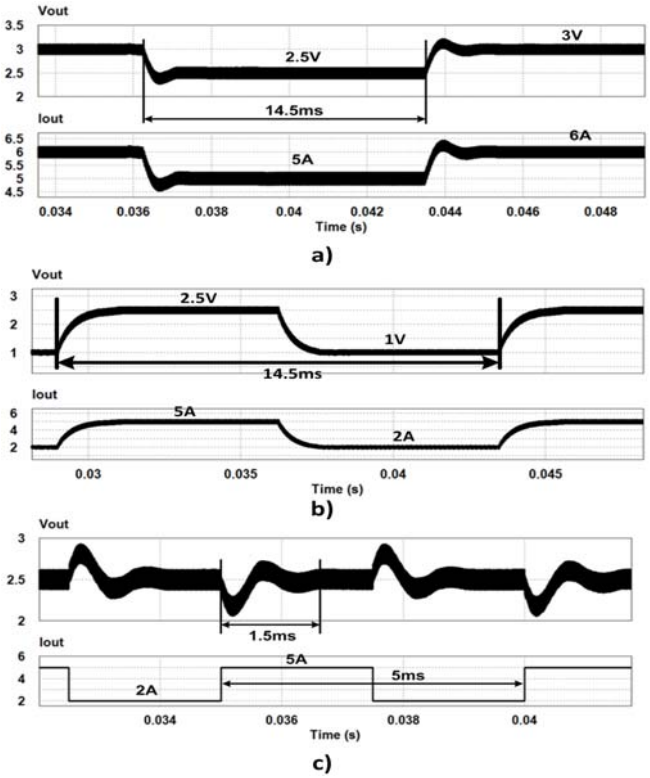

Figure 5. Simulation results for the average current mode control method implemented on the synchronous step down converter used to deliver power to the vaporizer filament for: a) current loop reference changed through software from 5A to 6A; b)voltage loop reference changed through software from 1V to 2.5V; c) output load change from 2A to 5A.

Three cases were tested and for each case the output voltage and output current of the converter are presented at: a) current reference step change; b)voltage reference step change; c) output load change.

An electronic load was used instead of the metal filament because only the average current mode control needs to be verified in the power stage design step.

The next step in the implementation of the temperature control system is to use the designed power stage with the temperature control algorithm.

IV. Temperature Algorithm Implementation

The algorithm was tested using PSIM power electronics dedicated software. The control algorithm was implemented in a 320F28027 microcontroller from TI simulated in PSIM with a generic microcontroller using C code. Because the simulation time increased significantly taking into account that the temperature process is very slow compared to the switching period, a macromodel has been proposed. The macromodel is used to test the algorithm with different types of filaments. The filament is represented by a nonlinear element that accepts a voltage-current relation. The voltage-current equation is determined for each filament based on the characteristics obtained experimentally. This macromodel is presented in Fig. 7, where the SMPS and the current loop that can be observed on the left side, are replaced with a voltage controlled current source, I_source.

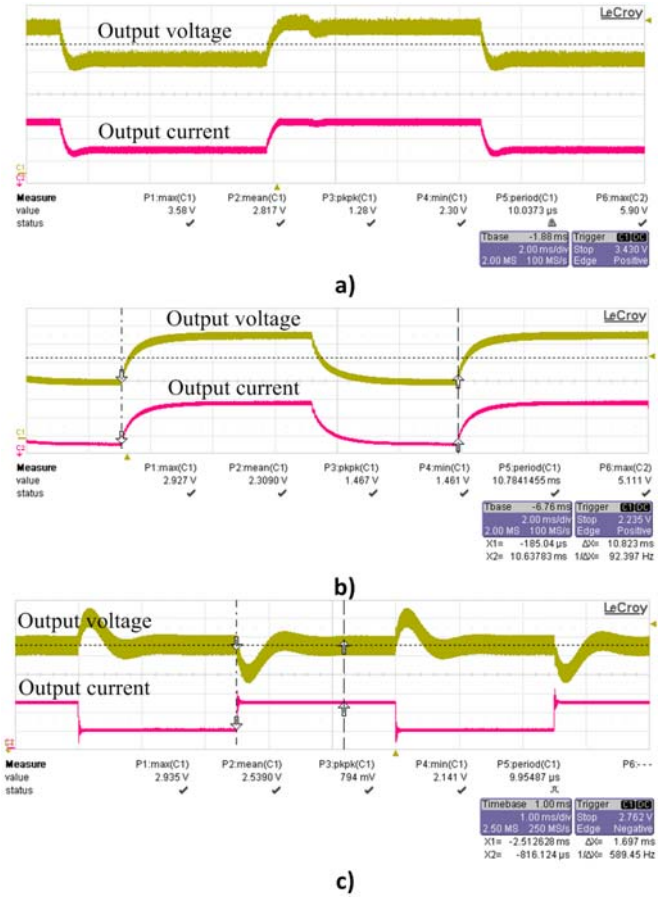

Figure 6. Experimental results for the average current mode control method implemented on the synchronous step down converter used to deliver power to the vaporizer filament for: a) current loop reference changed through software from 5A to 6A; b)voltage loop reference changed through software from 1V to 2.5V; c) output load change from 2A to 5A.

The fixed step temperature control algorithm was tested using the macromodel and the digital implementation of the control loops. In Fig. 8 the digital implementation of the PI voltage loop controller is presented. The controller was obtained transposing the analog implementation into the discrete domain using the Z transform. The error signal is obtained from the difference between the set point value and the process variable value sampled with the switching period. The set point is a digital value saved in the microcontroller's memory and updated from the PC based user interface. The value represents the voltage reference and is incremented or decremented with the step value according with the filament resistance comparison result. The output of the digital voltage loop is the set point of the faster inner current loop also implemented in discrete domain based on a PI algorithm. The linear recursive equation that implements the discrete PI algorithm is presented in (2) and the coefficients can be identified in the block representation of the controller in Fig. 8. I_{ref} is the output of the voltage loop (the current set point value); $I_{ref}[n-1]$ is the current reference value computed one sampling period before (z^{-1} is a unit delay in the Z domain); A1 is the coefficient of the current reference past sample; ERR is the error signal computed based on the present value of the voltage reference; and B1, B2 are the coefficients of the present and past value of the error signal.

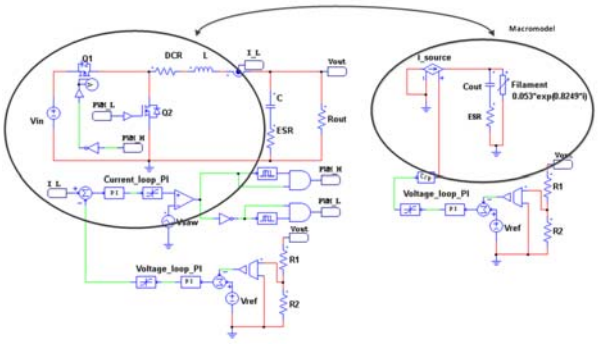

Figure 7. The schematics of the SMPS with the two control loops in analog domain and the macromodel used to test the algorithms.

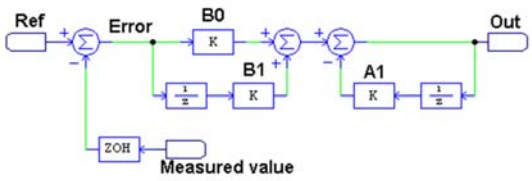

Figure 8. The digital implementation of a PI controller.

$$I_{ref}[n] = B_0 \cdot ERR[n] + B_1 \cdot ERR[n-1] - A_1 \cdot I_{ref}[n-1] \quad (2)$$

The temperature control algorithm implemented in the block C1 uses the SMPS output voltage and output current ratio averaged over 21 samples to compute the filament resistance. The computed resistance is compared to the reference value and the decision is made based on the comparison result. The reference value is delivered to the microcontroller from the computer interface. The filament resistance value, res_filament in Fig. 10, is computed with a 10 ms period and the voltage reference is incremented or decremented with a fix step if the steady state error is not zero. The fixed step value corresponds to a +/- 9.6 mV voltage change on the vaporizer filament, V_filament in Fig. 10, for a 12 bit ADC.

The value of the step is computed starting from the transfer characteristic of an ADC: $V_{num}=V_{IN}/V_{FS}$, where V_{IN} is the analog value, V_{num} is the value converted in digital format and V_{FS} is the full scale voltage of the converter. The converter used has a full scale voltage of 3.3 V and the result can be represented on 12 bits, resulting an absolute resolution ($R_{abs}=V_{FS}/(2^n-1)$), of 805µV, where 2^n is the maximum number of values that V_{num} can take. Using the resolution value and taking into account the gain of the voltage divider K_{div} used to sense the output voltage, the algorithm step will be $V_{step}=R_{abs}*step*1/K_{div}$. For a gain of 0.5 and a step value of 6 the voltage step value is $V_{step}=9.6mV$.

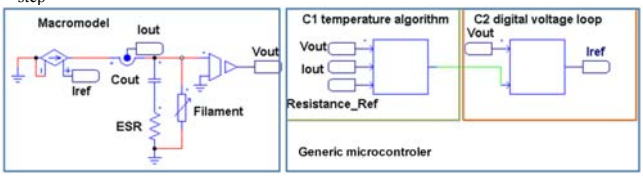

Figure 9. The schematic used to test the temperature control algorithm.

The simulation results of the temperature control algorithm for a temperature set point change between two values are shown in Fig. 10. The resistance set point value is modeled in the simulation with a square wave voltage source, where the signal values of the source are the

resistance values corresponding to 251˚C and 191˚C filament temperature. The resistance values, Res_ref in Fig. 10, are computed based on the resistance-temperature characteristic of the Rh filament.

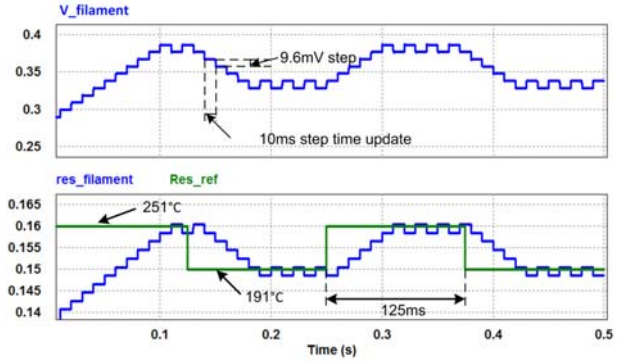

Figure 10. The output voltage of the filament at resistance set point change and the resistance controlling algorithm.

From Fig. 10 one can observe the time between two algorithm steps, 10 ms, and also the output voltage step of 9.6 mV corresponding to a change in the voltage set point of digital value 6. The resistance set point change corresponds to 60˚ C change with a 250ms period.

Based on the simulation results the algorithm was implemented using a 320F28027 Piccolo microcontroller from TI and the results are presented in the next section.

V. Experimental Results

The characteristic equation resistance as a function of temperature, $R_{filament}$=f(T°C), or voltage as a function of temperature for different materials (Rh, Pt and Au) can be determined based on experimental measurements.

The evaporator filament presented in Fig. 11 has 4 turns made of Rhodium (Goodfellow, England) of 99.99% purity with 0.25mm diameter and 29mm length ($\Phi_{interior}$: 2mm). The filament is fixed with two Molybdenum capillaries in a Teflon stand as presented in Fig. 11. During the atomization process the filament is introduced into the T form quartz tube that has an inner diameter of 6mm. Rhodium is a metal appropriate for high temperature applications (1900 degrees melting point temperature) that permits probe evaporation temperatures of 1500˚C.

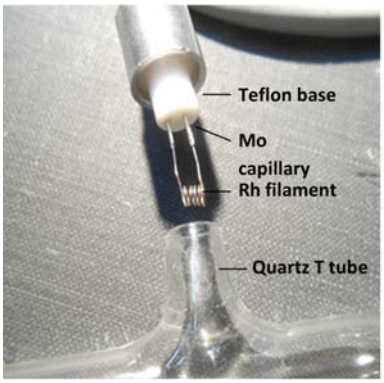

Figure 11. Experimental setup of the Rh filament.

The measured data for different types of filament materials were used to compute the voltage-temperature, current-temperature and resistance-temperature characteristics equations.

In Fig.12a the resistance-temperature characteristic of a rhodium filament is presented and in Fig. 12b the filament image in IR is recorded with a thermo vision camera. The filament resistance value at different temperature values was obtained based on the voltamperometric method by setting the voltage reference of the SMPS and measuring the current through the filament.

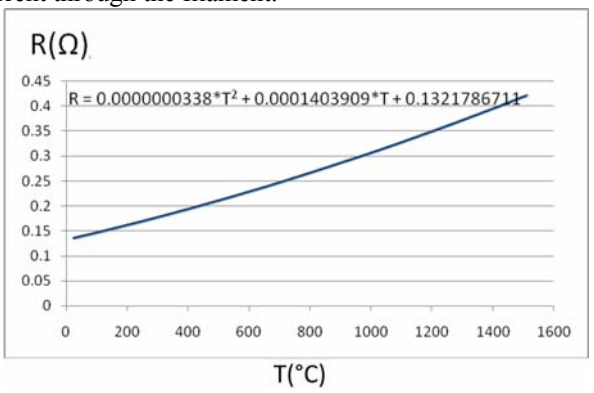

a)

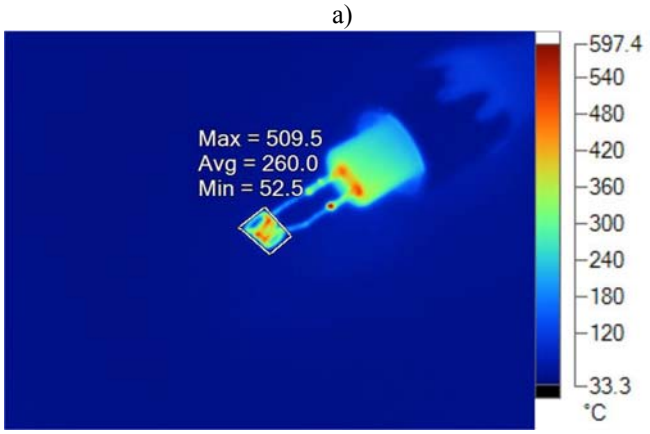

b)

Figure 12. a) Resistance-temperature characteristic of Rh filament; b) Infrared vision of the Rh filament.

In Fig. 13a the characteristic equation voltage as a function of temperature, $V_{filament}$=f(T°C), for Pt is presented and in Fig. 13b the filament image in IR is recorded with a thermo vision camera.

The equation was obtained from the data taken experimentally with a pyrometer.

They represent the linearized relation between two parameters (Resistance/Temperature for the Rh filament or Voltage/Temperature for the Pt filament) based on 20 measurements where R is in ohm, T is in degrees Celsius, I in Amps, U in volts. The data was introduced in excel and the appropriate interpolation to match the obtained points was used. The value obtained from the equation was used as reference for the control algorithm. This value is computed in a dedicated developed user interface where the user can choose between different evaporator material, time to run and temperature value to be set.

The equations (3-5) are used in the interface as presented but they can be changed after recalibration or if the evaporator physical characteristic is different from the one used in this example.

$$R_{Pt} = 0.0023454034 \cdot T + 0.0781823040 \quad (3)$$

$$R_{Rh} = 338 \cdot e^{-10} \cdot T^2 + 1403909 \cdot e^{-10} \cdot T + 0.1321786711 \quad (4)$$

$$R_{Au} = 0.003681 \cdot T + 0.9242 \quad (5)$$

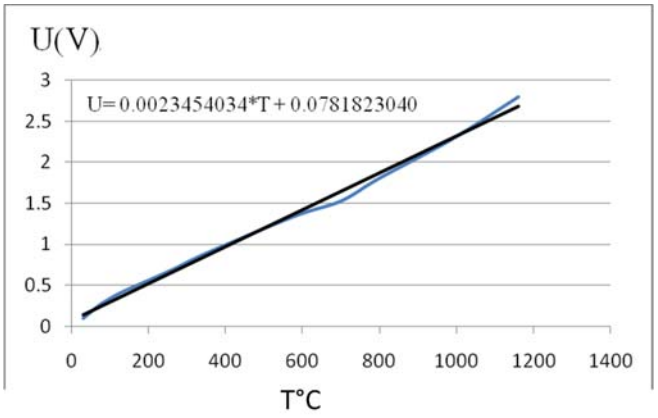

a)

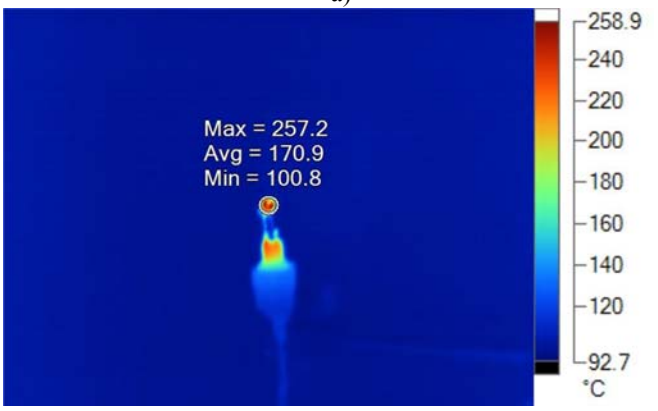

b)

Figure 13. a) Resistance-temperature characteristic of Pt filament; b) Infrared vision of the Pt filament..

The values of the coefficients are so small and with so many significant values because the difference in magnitude between the two values (temperature reaches 1000 degrees where the resistance is a value under unity). It is true that not all the coefficients need the same significant values, as it was stated that a voltage difference of micro volts cannot be compensated but the 10 significant values are relative to the smallest value for consistency.

An electronic board has been designed and assembled in order to implement the temperature control algorithm. The developed device can be divided into 4 blocks based on their functions as presented in Fig. 14.

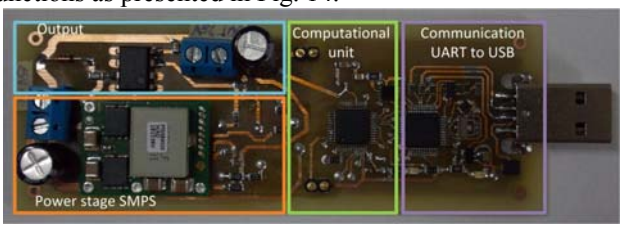

Figure 14. The vaporizer power supply designed to implement the temperature control algorithm.

The communication UART to USB block converts and transfers data between the microcontroller that implements the temperature control algorithm and the computer where the user interface is installed. The power stage is represented by a synchronous step down converter rated at 20W. The output block includes the low ESR output capacitor and the output voltage transducer.

In Fig. 15 the waveforms of the output voltage during the temperature set point tracking are presented. When a new resistance set point is received from the computer, the voltage set point is changed with +/- 9.6 mV each 10 ms until the output voltage-output current ratio is equal to the filament resistance corresponding to the desired temperature.

In Fig. 15a and 15b, 10 algorithm steps are presented. The two waveforms are compared in Fig. 15c and one can observe that the experimental result validates the new temperature control method proposed by the authors in this paper and the macromodel used in simulation to develop the algorithm for different types of metallic coils.

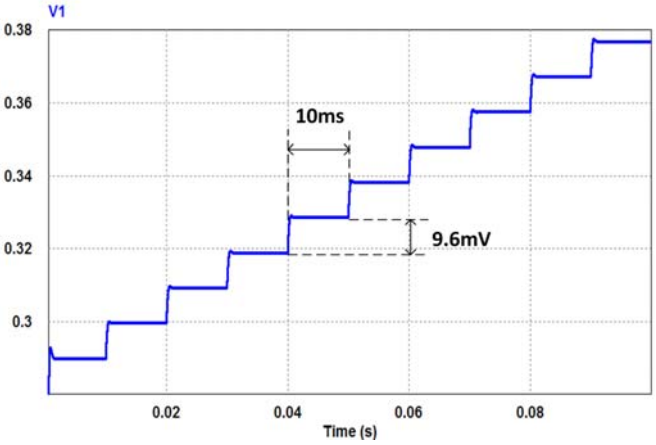

a)

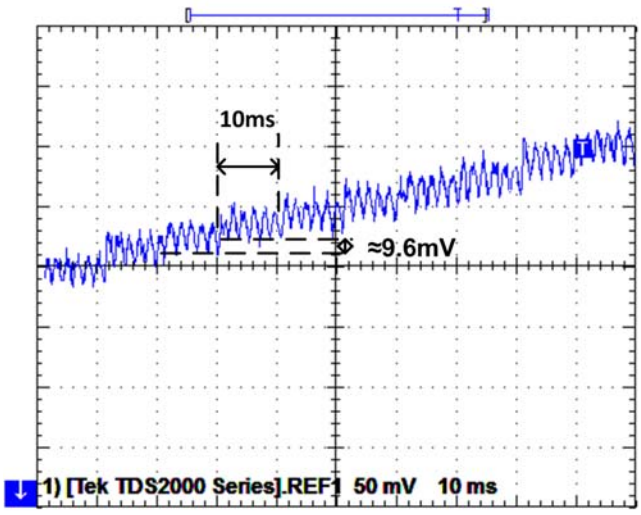

b)

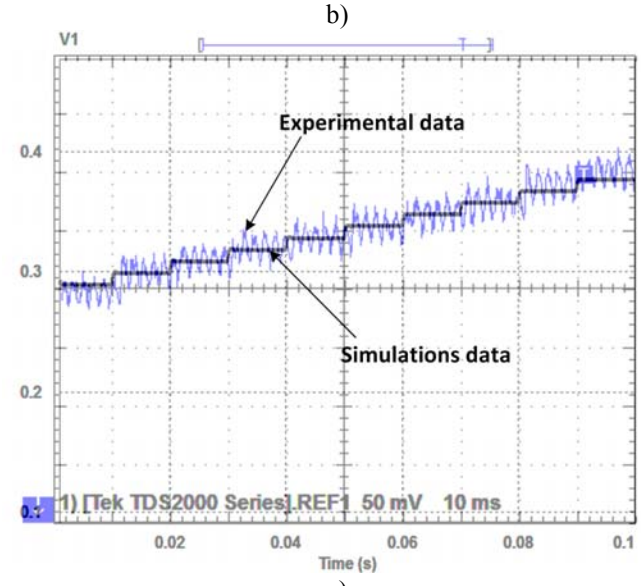

c)

Figure 15. Output voltage waveforms corresponding to: a) simulated; b) experimental; c) simulation and experimental overlapped.

VI. CONCLUSIONS

A device that implements the proposed indirect temperature control algorithm has been developed and tested with different metallic filaments Rh, Pt and Au.

The temperature control algorithm can be interpreted as a tracking algorithm. Based on the reference received from the dedicated user interface the microcontroller increases or decreases the voltage reference with a fixed step value until the ratio voltage-current reaches the steady state value.

Compared to the other temperature control algorithms found in literature, the proposed algorithm has the following advantages: it does not require a dedicated temperature sensor, it uses only two transducers, one for the output voltage and one for the inductor current, it has greater immunity to noise, it can be used with different types of metallic filaments, it can be used for applications that need high temperature values and the device that implements the algorithm has a small volume and low power consumption. The filament current measurement is obtained from the average value of the inductor current thus it is not needed an auxiliary current transducer.

The power consumption of the device depends on the filament used. For example the Rh filament needs 10.5W to reach 1500°C and 0.55W for 100°C. The buck converter is a switch mode power supply with high efficiency 96% and the Piccolo microcontroller is a low power device with a power consumption of maximum 400 mW. The maximum power consumed can reach 13~15 W in worst cases.

The temperature control approach can work in the range of 50-1500°C as long as the material supports that temperatures and the calibration process is correctly accomplished. The low temperatures accuracy depends on the material and the design of the filament. For the in the laboratory designed Rh filament the temperature range was 80-1700°C. Because the approach uses the voltage and current measurement to control the temperature, the maximum temperature does not limit the use of the new method proposed by the authors in this paper.

ACKNOWLEDGMENT

This work was supported by a grant of the Romanian National Authority for Scientific Research, CNDI–UEFISCDI, project number PN-II-PT-PCCA-2011-3.2-0219 (Contract no. 176/2012).

REFERENCES

[1] J. A. Rust, G. I. Donati, M. T. Afonso, J. A. Nobrega, B. T. Jones, "An overview of electrothermal excitation sources for atomic emission spectrometry", Spectrochim, Acta Part B, vol. 64, nr. 3, pp. 191-198, 2009. [Online]. Available: http://dx.doi.org/10.1016/j.sab.2009.02.003.

[2] D. J. Butcher, "Advances in electrothermal atomization atomic absorption spectrometry: instrumentation, methods and applications", Appl. Spectrosc. Rev., 41, pp. 15-34, 2006. [Online]. Available: http://dx.doi.org/10.1080/05704920500385460.

[3] S.d.L. - V. Maestre, M.T.C., "Plasma behavior during electrothermal vaporization sample introduction in inductively coupled plasma atomic emission spectrometry", Spectrochimica Acta Part B, 56, pp. 1209-1217, 2001. [Online]. Available: http://dx.doi.org/10.1016/S0584-8547(01)00218-X.

[4] B. Hu, S. Li, G. Xiang, M. He, Z. Jiang, "Recent progress in electrothermal vaporization-inductively coupled plasma atomic emission spectrometry and inductively coupled plasma mass spectrometry", Applied Spectroscopy Reviews, 42, pp. 203-234, 2007. [Online]. Available: http://dx.doi.org/10.1080/05704920601184317.

[5] J. H. Fujiyama-Novak, C. K. Gaddam, D. Das, R. L. Vander Wal, B. Ward, "Detection of explosives by plasma optical emission spectroscopy", Sensors and Actuators B: Chemical, 176, pp. 985-993, 2013. [Online]. Available: http://dx.doi.org/10.1016/j.snb.2012.08.063.

[6] Summer N. Hanna, Clifton P. Calloway Jr., Jason D. Sanders, Ronald A. Nelson, "Design of a compact, aluminum, tungsten-coil electrothermal vaporization device for inductively coupled plasma-optical emission spectrometry", Microchemical Journal, 99, pp. 165-169, 2011. [Online]. Available: http://dx.doi.org/10.1016/j.microc.2011.04.009.

[7] X. Wen, P. WU, L. Chen, X. Hou, "Determination of cadmium in rice and water by tungsten coil electrothermal vaporization-atomic fluorescence spectrometry and tungsten coil electrothermal absorption spectrometry after cloud point extraction", Analytica Chimica Acta, 650, pp. 33-38, 2009. [Online]. Available: http://dx.doi.org/10.1016/j.aca.2009.01.053.

[8] Bings, N. H. S., Z. Stefanka, "Development of a tungsten filament electrothermal vaporizer for inductively coupled plasma time-of-flight mass spectrometry and its possibilities for the analysis of human whole blood and serum", Journal of Analytical Atomic Spectroscopy, 18, pp. 1088-1096, 2003. [Online]. Available: http://dx.doi.org/10.1039/b301950k.

[9] X. Huo, B. T. Jones, "Field instrumentation in atomic spectroscopy", Microchem. J., 66, pp. 115-145, 2000. [Online]. Available: http://dx.doi.org/10.1016/S0026-265X(00)00058-8.

[10] S. N. Hanna, J. Keene, C. P. Calloway, B. T. Jones, "Design of a Portable Electrothermal Vaporization Flame Atomic Emission Spectrometry Device for Field Analysis, Instrumentation Science and Technology", 39(4), pp. 345-356, 2011. [Online]. Available: http://dx.doi.org/10.1080/10739149.2011.585197.

[11] X. Hou, K. E. Levine, A. Salido, B. T. Jones, M. Ezer, S. Elwood, J. B. Simeonsson, "Tungsten coil devices in atomic spectrometry: absorption, fluorescence, and emission", Analytical Sciences, 17, pp. 175-180, 2001. [Online]. Available: http://dx.doi.org/10.2116/analsci.17.175.

[12] C. L. Sanford, S. E. Thomas, B. T. Jones, "A portable, battery-powered, W coil atomic absorption spectrometer for Pb determinations", Appl. Spectrosc., 50, pp. 174-181, 1996. [Online]. Available: http://dx.doi.org/10.1366/0003702963906591.

[13] Z. F. Queiroz, P. V. Oliveira, J. A. Nobrega, C. S. Silva, I. A. Rufini, S. S. Sousa, F. J. Krug, "Surface and gas phase temperatures of a tungsten coil atomizer", Spectrochim. Acta Part B, 57, pp. 1789-1799, 2002. [Online]. Available: http://dx.doi.org/10.1016/S0584-8547(02)00146-5.

[14] A. Virgilio, C. K. Healy, J. A. Nobrega, B. T. Jones, G. L. Donati, "Evaluation of atomizer conditioning and pyrolysis and atomization temperature control to improve procedures based on tungsten coil atomic emission spectrometry", Microchemical Journal, 110, pp. 758-763, 2013. [Online]. Available: http://dx.doi.org/10.1016/j.microc.2013.08.014.

[15] K. Levine, K. A. Wagner, B. T. Jones, "Low-cost, modular electrothermal vaporization system for inductively coupled plasma atomic emission spectrometry", Appl. Spectrosc., 52, pp. 1165-1171, 1998. [Online]. Available: http://dx.doi.org/10.1366/0003702981945174.

[16] S. N. Hanna, C. P. Calloway Jr., J. D. Sanders, R. A. Nelson, J. Cox, B. T. Jones, "Design of a compact, aluminum, tungsten-coil electrothermal vaporization device for inductively coupled plasma-optical emission spectrometry", Microchemical Journal, 99, pp. 165-169, 2011. [Online]. Available: http://dx.doi.org/10.1016/j.microc.2011.04.009.

[17] J. A. Rust, J. A. Nobrega, C. P. Calloway Jr., Bradley T. Jones, "Tungsten coil atomic emission spectrometry", Spectrochimica Acta Part B, 61, pp. 225-229, 2006. [Online]. Available: http://dx.doi.org/10.1016/j.sab.2005.12.009.

[18] S. Hanna, B. T. Jones, "An electrothermal vaporization flame atomic emission spectrometer", Journal of Analytical Atomic Spectrometry, 7 (26), pp. 1428-1433, 2011. [Online]. Available: http://dx.doi.org/10.1039/c1ja10060b.

[19] T. Patarau, D. Petreus, R. Etz, C. Orian, E. Darvasi, T. Frentiu, "Study and implementation of a vaporizer used in plasma equipment for heavy metals detection", IEEE 19th International Symposium for Design and Technology in Electronic Packaging (SIITME), 2013. [Online]. Available: DOI: 10.1109/SIITME.2013.6743655.

[20] R. Etz, D. Petreus, T. Frentiu, T. Patarau, "A digitally controlled programmable power supply used in a vaporizer", 36th International

Spring Seminar on Electronics Technology (ISSE), 2013. [Online]. Available: DOI: 10.1109/ISSE.2013.6648248.

[21] D. Draghici, D. Lascu, "Predictive Trailing-Edge Modulation Average Current Control in DC-DC Converters", Advances in Electrical and Computer Engineering (AECE), vol. 13, no. 4, pp. 111-116, 2013. [Online]. Available: DOI: 10.4316/AECE.2013.04019.

[22] C. Petrea, "Digital Control of Boost PFC Converter Working in Discontinuous Conduction Mode", Advances in Electrical and Computer Engineering (AECE), vol. 7, no. 2, pp. 16-19, 2007. [Online]. Available: DOI: 10.4316/AECE.2007.02004.

[23] R. Etz, T. Patarau, D. Petreus, S. Daraban, D. Moga, "Digital Control for Phase Shift Converter", IEEE International Conference on Automation, Quality and Testing, Robotics, 2012, ISBN: 978-1-4673-0701-7. [Online]. Available: http://dx.doi.org/10.1109/aqtr.2012.6237676.

[24] D. Maksimovic and R. Zane, "Small signal discrete-time modeling of digitally controlled DC-DC converters", Proc. IEEE Comput. Power Electron. (COMPEL), pp. 231-235, 2006. [Online]. Available: http://dx.doi.org/10.1109/compel.2006.305680.

[25] V. Yousefzadeh, A. Babazadeh, B. Ramachandran, E. Alarcon, L. Poa, D. Maksimovic, "Proximate time-optimal digital control for synchronous buck DC-DC converters", IEEE Trans. Power Electron., 23(4), pp. 2018-2026, 2008. [Online]. Available: http://dx.doi.org/10.1109/TPEL.2008.924843.